Journal of Catalysis 258 (2008) 356–365

Contents lists available at ScienceDirect

Journal of Catalysis

www.elsevier.com/locate/jcat

Effect of nickel microstructure on methane steam-reforming activity of Ni–YSZ cermet anode catalyst

David L. King *, James J. Strohm, Xianqin Wang, Hyun-Seog Roh, Chongmin Wang, Ya-Heui Chin, Yong Wang, Yuanbo Lin, Robert Rozmiarek, Prabhakar Singh

Institute for Interfacial Catalysis, Pacific Northwest National Laboratory, Richland, WA 99352, USA

ARTICLE INFO

Article history:
Received 8 May 2008
Revised 25 June 2008
Accepted 27 June 2008

Keywords:
Methane reforming
Ni–YSZ
Anode
Solid oxide fuel cell
Sintering
Exolution
Ni microstructure

ABSTRACT

The activity of nickel–yttria stabilized zirconia (Ni–YSZ) solid oxide fuel cell (SOFC) cermet anodes for the steam-reforming of methane has been investigated in the absence of electrochemical effects. The cermet was prepared by co-milling and sintering NiO and 5YSZ powders at 1375 °C in air. During the high-temperature sintering step, NiO dissolved into the YSZ particles to form a solid NiO–YSZ solution. During the subsequent catalyst reduction step, Ni exolved from the YSZ. As a result, many small Ni particles on the order of 10–20 nm formed at the surface of the YSZ. These small particles contributed significantly to the overall reforming activity, along with the large bulk Ni particles within the Ni–YSZ cermet. We observed high initial activity that decreased by as much as an order of magnitude with time on stream, until the anode catalyst reached a stable steady-state activity. The time to reach this stable activity was a function of the pretreatment and reaction conditions. Initial and lined-out activities and average turnover frequencies were obtained for both Ni–YSZ and bulk Ni, based on a rate expression that was first-order in methane and zero-order in steam. Comparative tests at 750 °C showed high initial activity on a per-Ni site basis with both materials, but these turnover rates declined over a period of a few hours. After lineout, there appeared to be a negligible effect of Ni particle size on turnover rate. These results indicate the presence of structure-sensitivity for methane reforming, but only with freshly calcined and reduced catalysts that may contain highly coordinatively unsaturated sites. There was an apparent structure-insensitivity with aged catalysts in which Ni particle sizes were generally $\geqslant$30 nm. Under reaction conditions with high space velocities and low methane conversions, the water–gas shift reaction did not establish thermodynamic equilibrium.

1. Introduction

Internal (endothermic) reformation of methane continues to be a topic of much interest in power generation from solid oxide fuel cells (SOFCs), due to its potential to increase the overall system efficiency, minimize reforming components, and provide effective cooling. Direct utilization and operation of a high temperature tubular SOFC with hydrocarbon fuel such as methane or synthetic natural gas, without the use of an external reformer, was experimentally demonstrated by Singh et al. [1]. Much of the published work in this area has focused on two general challenges: (i) avoiding carbon formation and (ii) moderating the reforming rate to avoid large thermal gradients along the anode flow direction [2,3]. For the former, the operating steam/carbon ratio plays an important role. In addition, alternative anode compositions have been described that may show promise for operating at relatively low S/C ratios (S/C $<$ 1) [4–6]. For thermal control, various approaches have been proposed, including modifying the porosity of the cell to control mass transfer of reactants [7], incorporating diffusion barriers or compositional gradients [8], and using additives such as copper to mediate the activity of the Ni catalyst [9].

Although thermal management of the anode operating on methane is critical for efficient and durable operation, there appears to be relatively little experimental work describing the operation of a SOFC with continuous monitoring of both the reformate composition and thermal profile at various axial locations along the anode. A primary reason for this is the cost and complexity of constructing such a well-instrumented device. As a result, computational modeling has become an important methodology for predicting conversion profiles versus distance [10,11] and thermal profiles or other performance metrics of a SOFC anode operating on methane or natural gas [12–16]. Internal reforming involves the conversion of the hydrocarbon fuel to syngas coupled with the electrochemical oxidation of the H_2 and CO produced. These individual steps can be treated separately by modeling; therefore, steam reforming of methane over the anode "catalyst" in the absence of electrochemical activity ("open circuit") can provide ki-

* Corresponding author. Fax: +1 509 375 2186.
E-mail address: david.king@pnl.gov (D.L. King).

0021-9517/$ – see front matter
doi:10.1016/j.jcat.2008.06.031

netic parameters to the model. It is important to obtain intrinsic kinetics, which can then be combined with heat and mass transfer effects to predict observable performance.

Numerous studies on the catalytic reforming activity of nickel–yttria stabilized zirconia (Ni–YSZ) and other anodes have been published [12,17–21]. However, significant disparities are seen in the rate expressions, rate constants, and activation energies. Moreover, the results from these studies are sometimes difficult to interpret, because the activity may be based on the geometric surface area of the anode rather than on a more fundamental property, such as the available metal surface area or weight of the active metal component. In addition, differences in preparation methods, compositions, and surface area and porosity can make it difficult to compare one set of results with another.

We initiated these studies to provide kinetic information on methane steam reforming with Ni–YSZ anode materials currently under development at the Pacific Northwest National Laboratory. Using an anode-supported cell, the anode comprises a porous bulk layer (500 μm thick; 40 vol% Ni) and an active layer (50 μm thick, 50 vol% Ni) in contact with the YSZ electrolyte. In addition to the nickel content, the two layers differ in that the bulk layer contains 5 mol% yttria (5YSZ), whereas the active layer contains 8 mol% yttria (8YSZ). We used the bulk anode formulation in our tests, because this is where the internal reforming occurs.

Our approach was to test the Ni–YSZ anode material as a catalyst powder. We tested the materials at high space velocities in an effort to measure conversion far from equilibrium, allowing us to more readily measure kinetic parameters and observe any deactivation effects. We found that the catalytic activity of freshly calcined and reduced Ni–YSZ is not stable, and that activity may decline over several to tens of hours. We also found that the reforming performance is a combined function of two types of nickel. The first type is derived from the bulk NiO present in the initial raw material, which consists of relatively large particles ($\geqslant$0.3–2.0 μm in diameter). The second is nanostructured Ni, which evolves from YSZ during pretreatment and is in the range of 10–20 nm. Both Ni types contribute significantly to the overall activity, and both undergo sintering during the reforming reaction, leading to a decline in reforming activity with time. Apparently, little information on this deactivation phenomenon for Ni–YSZ materials has been reported to date [22].

The work described in this paper is part of a larger study of the catalytic activity and activity maintenance of Ni–YSZ for methane steam reforming. The focus is on the development of a specific Ni microstructure that results from a reductive pretreatment using a temperature ramping procedure. Subsequent papers will describe the effect of alternate pretreatment methods on nickel microstructure development, and performance of a Ni–YSZ wafer in a plate reactor.

2. Experimental

2.1. Materials preparation

The Ni–YSZ SOFC anode material tested is based on that used in an anode-supported cell. The anode comprises a thin active layer (10 μm thick, 50 vol% Ni–8YSZ) and a bulk anode (500 μm thick, 40 vol% Ni–5YSZ). On reduction, the bulk anode is approximately 50% Ni by weight. The compositions used in our tests were of the bulk anode only. The bulk anode was prepared from NiO (Baker, electronic grade) and 5YSZ (Unitek HSY8, 5 mol% Y_2O_3) powders. The powders were first co-milled in an attrition mill using isopropanol as solvent to a particle size specification. Typically, the resulting powder was tape cast to form a wafer, using isopropanol (reagent grade) as a solvent and carbon as a pore-former. This material was subsequently fired in air using a temperature ramp of 5 °C/min to 1375 °C, with a hold for 1 h. These materials were subsequently ground for reactor testing in a mortar and pestle. We also tested powders simply taken after the milling process and calcined using the same protocols without the tape casting and forming steps. We found virtually no difference in the performance from the samples obtained from these two preparation methods, and most of the studies used the materials prepared by the latter method. The BET surface area of the calcined Ni–YSZ was 0.45 m^2/g, which increased to 1.1 m^2/g following reduction (see below).

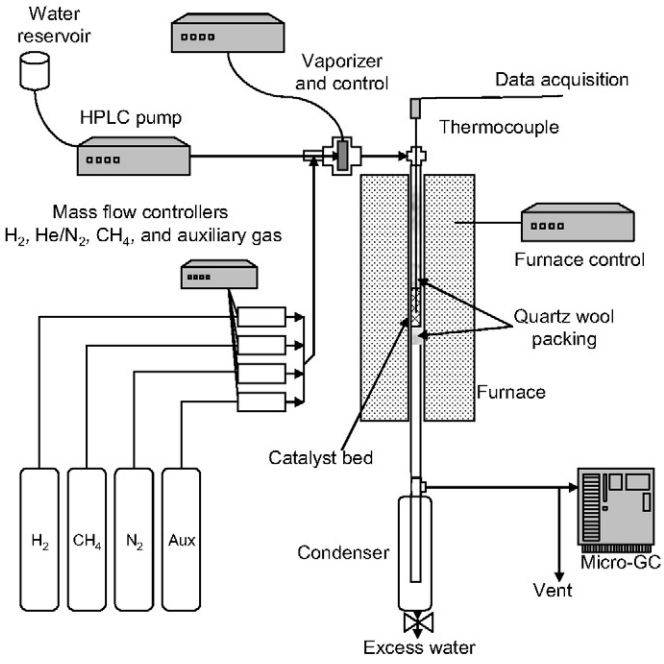

Fig. 1. Reactor schematic.

2.2. Catalytic testing

A schematic of the test apparatus is shown in Fig. 1. The Ni–YSZ material was ground with a mortar and pestle and a sample of 100–200 mesh (75–150 μm) was used for all tests. A further reduction in particle size did not result in a change in catalyst performance, consistent with the absence of intraparticle mass transfer limitations. We typically used a 20–50 mg sample diluted 10× (by wt.) with YSZ, loaded into a small tubular reactor and secured by quartz wool packing. Packing density of the catalyst plus YSZ diluent was 0.485 g/cm^3. Both a 9-mm-i.d. quartz tube (catalyst bed length, 8 mm) and a 6.5-mm-i.d. inconel tube (bed length, 11 mm) were used and provided quite similar results. The catalyst reactor tube was heated by a small tube furnace. A thermocouple that could be placed at different locations within the catalyst bed was used to monitor the catalyst temperature.

Catalyst pretreatment involved a ramped reduction in hydrogen from ambient to the final reaction temperature (generally 700 °C), with a hold at that temperature for 1 h. Various ramp rates were used for the reduction, from 5 to 20 °C/min, but this appeared to have minimal effect on the performance of the catalyst. After reduction, the H_2 and inert flows were adjusted and steam was introduced for at least 15 min before the addition of CH_4.

Reactant feed to the system comprised CH_4 (Matheson, UHP), H_2 (Matheson, UHP), and deionized H_2O, frequently diluted with He or N_2 to allow the concentration of one of the components to be varied while maintaining a constant space velocity. H_2O was vaporized and mixed with the gas feeds upstream of the reactor. In the early stages of the work, precautions were taken to rigorously

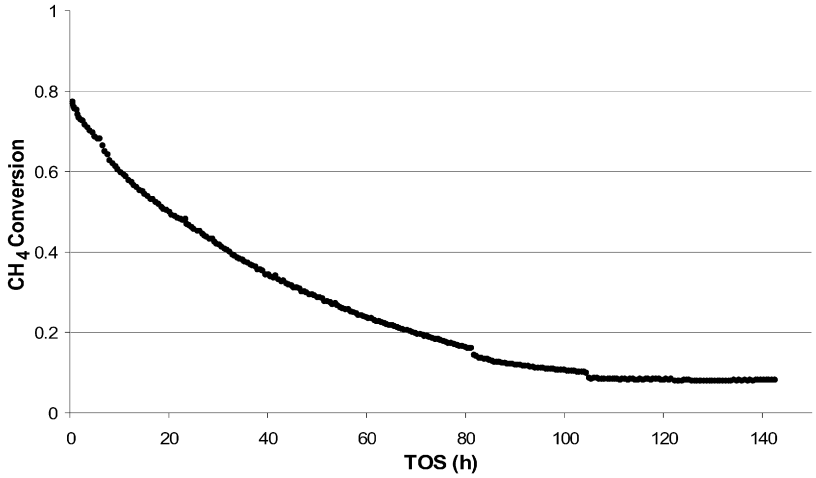

Fig. 2. CH_4 conversion vs time on stream for Ni–YSZ reduced at 700 °C. Test conditions: $T = 700$ °C; S/C/H/He = 3/1/1/5; SV = 667,000 cc/g h (48 g CH_4/g h).

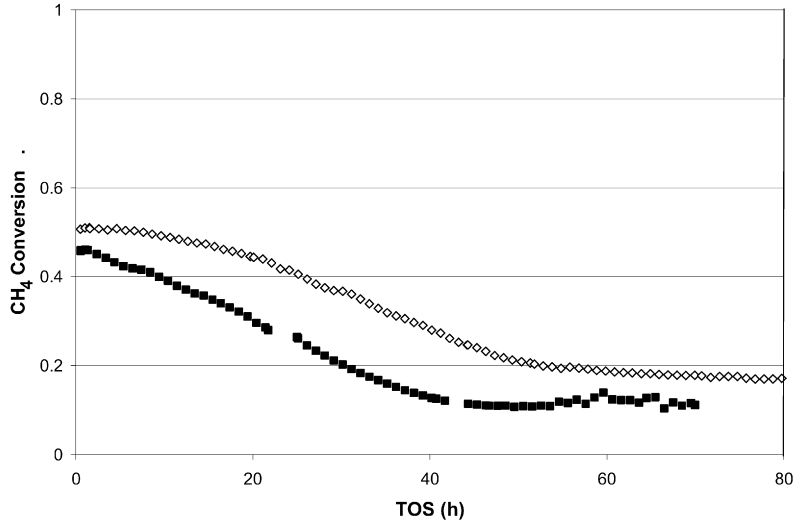

Fig. 3. Effect of reduction conditions on subsequent catalytic activity at 700 °C. (◇) Reduction at 750 °C in 3% H_2O/97% H_2, 159 h; (■) reduction at 1000 °C, 4 h. Test conditions: $T = 700$ °C; S/C/H = 3/1/1; SV = 342,000 cc/g h (48 g CH_4/g h).

exclude H_2S from the feed using commercial sulfur traps. No difference in catalytic performance was observed compared with the trap-free system, so the cylinder gases were subsequently used as received. Feed composition typically was set at a $H_2O/CH_4/H_2/N_2$ ratio of 3/1/1/1. Typical feed rates of 0.12 cc (liq)/min for H_2O and 45 cm^3/min for each of the gases provided a WHSV (CH_4) of 49 g/g_{cat} h (GHSV 324 K cc/g_{cat} h) although other conditions were sometimes used and noted accordingly. Reaction products were analyzed online using a Hewlett Packard micro-GC, with a dual TCD detector. Analysis for H_2, CO, CH_4, and N_2/He used a molecular sieve A column (Ar carrier gas), and analysis for CO_2 used a PlotU column (He carrier gas).

Despite high catalyst dilution with YSZ and reactant dilution with inert gas, we nevertheless measured an endotherm of 20–30 °C in the front part of the catalyst bed, even though the middle and exit bed temperatures were at the nominal temperature reported. Tests in which the catalyst charge was varied while maintaining constant space velocity provided very similar CH_4 conversion values, consistent with the absence of nonintraparticle mass transfer limitations.

2.3. Materials characterization

X-ray (XRD) characterization was carried out using a Philips wide-range vertical goniometer. A wide-range scan was performed on all samples using a 2θ step of 0.05° from 20 to 85° with 1-s steps. For detailed quantification of the $(111)_{c,t}$ zirconia peak, a high-resolution scan from 20 to 36° was performed using a 2θ step of 0.02° and a 5-s dwell.

Samples for TEM analysis were prepared by pressing finely ground powders onto an Au grid. HRTEM analysis was carried out on a Jeol JEM 2010F microscope with a specified point-to-point resolution of 0.194 nm. An operating voltage of 200 keV was used, and all images were digitally recorded with a slow scan charge-coupled device camera. Qualitative atomic compositions were determined by EDS analysis performed on a Vacuum Generators HB603 scanning transmission electron microscope.

Pulsed H_2 chemisorption measurements were performed on a Micromeritics Autochem 2920 catalyst characterization system, using a 1-g sample loaded in a U-shaped quartz tube. Before chemisorption measurements, the sample was reduced in a 5% H_2/95% Ar atmosphere with a temperature ramp of 5 °C/min from room temperature to 700 °C with a hold for 1 h at 700 °C. Other reduction protocols were used to match the experimental conditions. After reduction, the sample was flushed with Ar flow for 1 h, then cooled to 45 °C. Quantitative pulses of hydrogen were then added until saturation was observed. The total hydrogen uptake was then used to calculate the amount of exposed Ni surface atoms assuming a 1:1 H:Ni adsorption ratio.

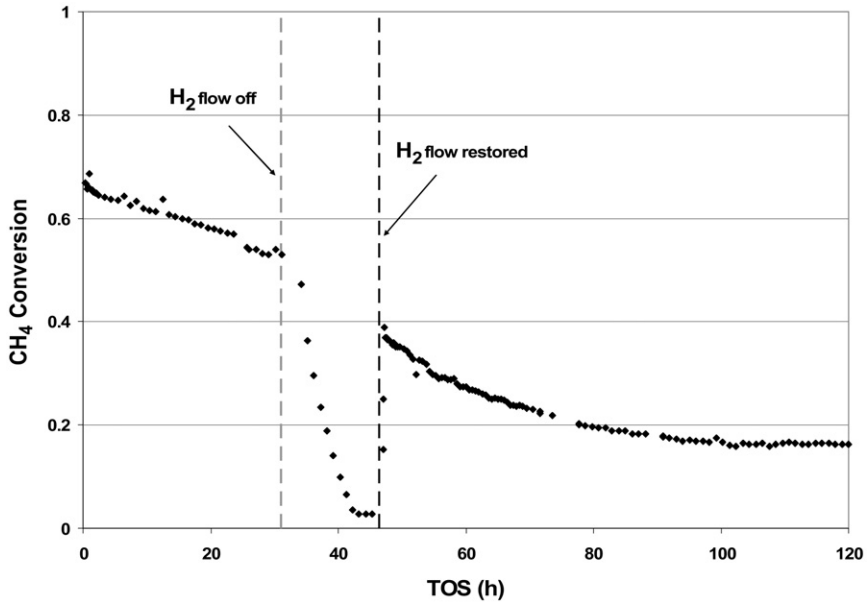

Fig. 4. Methane conversion over Ni–YSZ showing the effect of removing H_2 from feed. Test conditions: 700 °C, S/C/H/N = 3/1/1/5, SV = 684 K (48 g CH_4/g h).

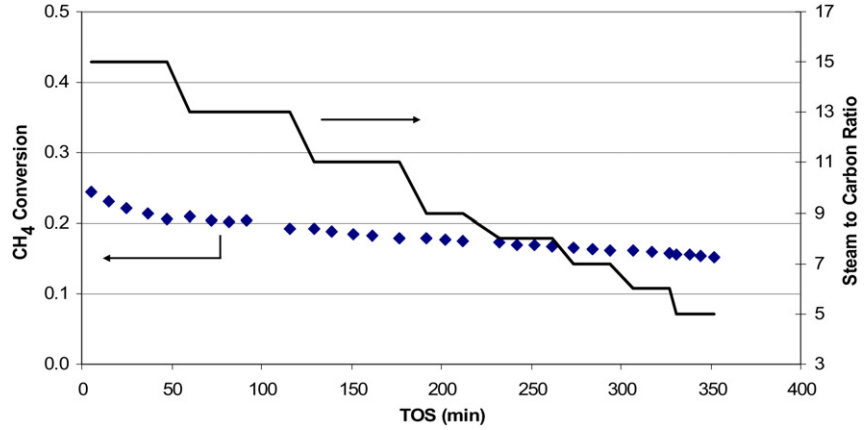

Fig. 5. CH_4 conversion vs time on stream for Ni–YSZ over a range of S/C ratios. Catalyst was pretreated in 5/1 H_2O/H_2 for 100 h at 700 °C followed by H_2 reduction at 700 °C. Test conditions: 700 °C, SV = 330,000 cc/g h, CH_4/H_2 = 10.

3. Results

3.1. Catalytic tests

Fig. 2 shows the methane conversion with time on stream at 700 °C for a diluted 30-mg sample of Ni–YSZ. The feed composition was S/C/H_2/He = 3/1/1/5, and the WHSV was 48 (g_{CH_4}/g_{cat} h). The conversion of CH_4 was initially high at 78% but decreased over a period of 120 h until leveling out at approximately 9%. Fig. 3 shows the results of reduction at the higher temperatures of 750 and 1000 °C, followed by the same activity test at 700 °C. Although the initial and lined-out activities show some variation, the same general trend of significant deactivation can be seen. The sample with the highest initial activity was produced by reduction at 700 °C. On post-test examination by TEM/EDS, none of the samples showed any evidence of carbon formation.

We proceeded to evaluate the effect of hydrogen concentration in the feed on performance. In the absence of H_2 in the feed, the nickel could be oxidized during steam reforming, thereby becoming inactive. This is shown in Fig. 4. On restoring the H_2 flow, activity increased rapidly due to re-reduction of the NiO to Ni, although not to the same activity level as before the H_2 flow was terminated. Thus, a co-feed of H_2 along with steam and methane was always used.

Although the evidence pointed toward Ni sintering to explain the loss in Ni–YSZ activity with time, we had difficulty in understanding how such a decrease in activity could arise given the large Ni particles used to generate the anode (typically 0.3–2.0 μm). Although an operating S/C ratio of 3 should maintain the catalyst free of carbon, we were concerned that carbon might still be depositing due to local feed inhomogeneities, thereby causing the deactivation. Fig. 5 shows the results of an experiment in which the S/C ratio was set initially at a very high ratio of 15/1 and subsequently lowered stepwise to a final value of 5/1. The catalyst was initially pretreated in an atmosphere of H_2O/H_2 of 1 for 100 h at 700 °C before being used for the test. Despite the long steaming pretreatment, a further gradual decrease in activity was observed during methane reforming. The initial high S/C ratio precluded the possibility that carbon formation was contributing to the observed deactivation profile.

Additional information can be gleaned from the experimental results shown in Fig. 5. The CH_4 and H_2O partial pressures were changed in stepwise manner (CH_4 from 0.16–0.06 atm; H_2O from 0.82–0.93 atm), with total flow rate and pressure held constant. A smooth, small continuous decline in methane conversion

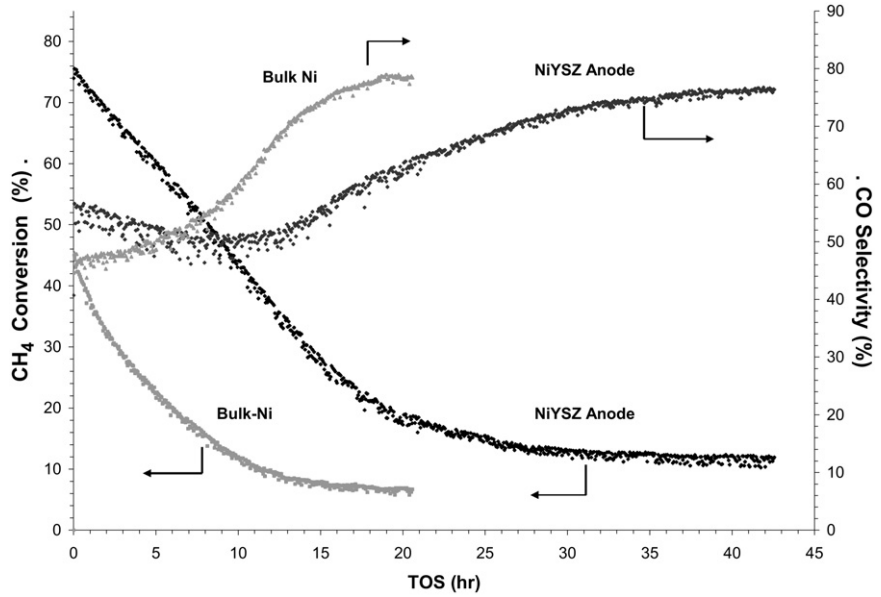

Fig. 6. Comparison of methane steam reforming activity between bulk Ni and Ni–YSZ using the same source and quantity of NiO. Test conditions: 750 °C, S/C/H/N = 3/1/1/1; Ni–YSZ: GHSV = 328,000 cc/g Ni h; bulk Ni: GHSV = 660,000 cc/g Ni h.

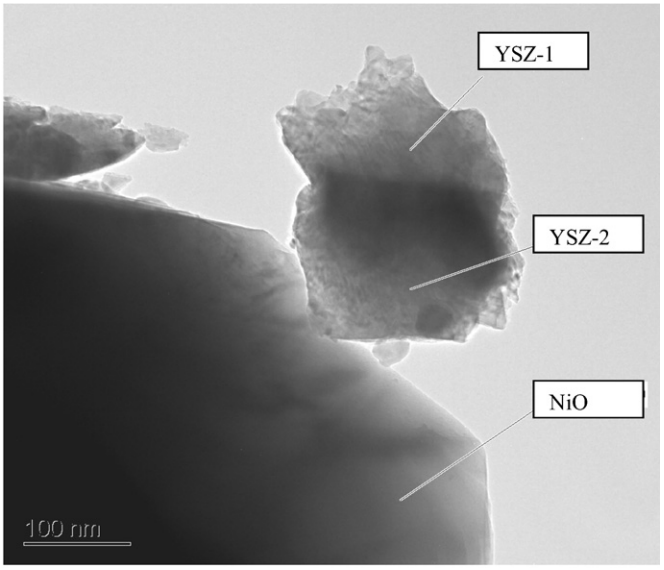

Fig. 7. TEM photograph of NiO and YSZ particles following calcination at 1375 °C showing location of EDS measurements.

was observed over the course of the test. Although not a rigorous demonstration of the effect of feed concentration on rate, the lack of discontinuity in the CH_4 conversion is consistent with a first-order dependence of the rate on CH_4 partial pressure. Moreover, the conversion trend as a function of steam partial pressure is inconsistent with the negative-order dependence with respect to H_2O concentration reported by others [18,23–25] and is more consistent with a zero-order dependence. In other experiments, we similarly found a zero-order dependence on H_2O concentration except at low H_2O concentrations ($S/C \leqslant 1$), where low H_2O partial pressures led to a decrease in CH_4 conversion. In subsequent activity calculations, we therefore assumed a rate expression that was first-order in methane and zero-order in H_2O.

All of these results indicate deactivation caused by loss of nickel catalytic activity through sintering, facilitated by steam and hydrogen and possibly also by methane. This phenomenon is well documented [26,27], although we have not seen a description of sintering behavior and time-dependent CH_4 conversion with respect to Ni/YSZ anode cermets. We then carried out a reactor test in which the NiO initial source material (without the YSZ) was evaluated for catalytic activity and lineout behavior and compared with Ni–YSZ performance at 750 °C (Fig. 6). This NiO sample (used without dilution) was calcined at 1375 °C in air and reduced in H_2 using a temperature ramp to 750 °C with a 1-h hold. For comparison with Ni–YSZ, the NiO sample used was half the weight of the Ni–YSZ (thus the same weight of Ni), and the test was carried out at the same WHSV based on Ni (weight CH_4 per weight Ni). It is notable that the bulk Ni sample also showed a substantial loss in activity with time, indicating that significant change in the Ni surface also must be occurring. The Ni–YSZ had greater activity than the bulk Ni sample on a per-weight-of-Ni basis, indicating that there must be some additional available nickel contributing to this activity difference. We discuss the CO selectivity, also shown for these two catalysts in Fig. 6, later in the paper.

3.2. Microstructural analysis

3.2.1. TEM–EDS analysis of as-received Ni–YSZ after high-temperature calcination

Fig. 7 shows a TEM image taken from a sample of Ni–YSZ cermet powder after high-temperature air calcination (sintering) at 1375 °C for 1 h. Both YSZ and NiO particles are shown. Many YSZ particles that we observed were larger than that shown in the figure; however, the particle shown here was selected because it was free of other overlapping particles. EDS analysis was conducted at the two locations on the YSZ particle, as indicated. Fig. 8 shows the EDS elemental traces for both the NiO and YSZ particles. The EDS spectrum of the NiO particle exhibits only nickel peaks. (The Au signal is due to the TEM grid used.) On the other hand, for the YSZ particle, the EDS spectra show that Ni (as the oxide) is also present. This result is quite typical; most of the YSZ particles that we examined showed some concentration of Ni associated with the YSZ, although there was some variation in the intensity of the Ni signal from particle to particle. Quantifying the amount of NiO present is difficult with this technique, but NiO certainly was present well above trace levels, most likely in the few percent range. There are two different possible explanations for these results: Either some fine NiO powder, generated through the milling procedure, was deposited on the surface of the YSZ particle or NiO was physically dissolved into the YSZ.

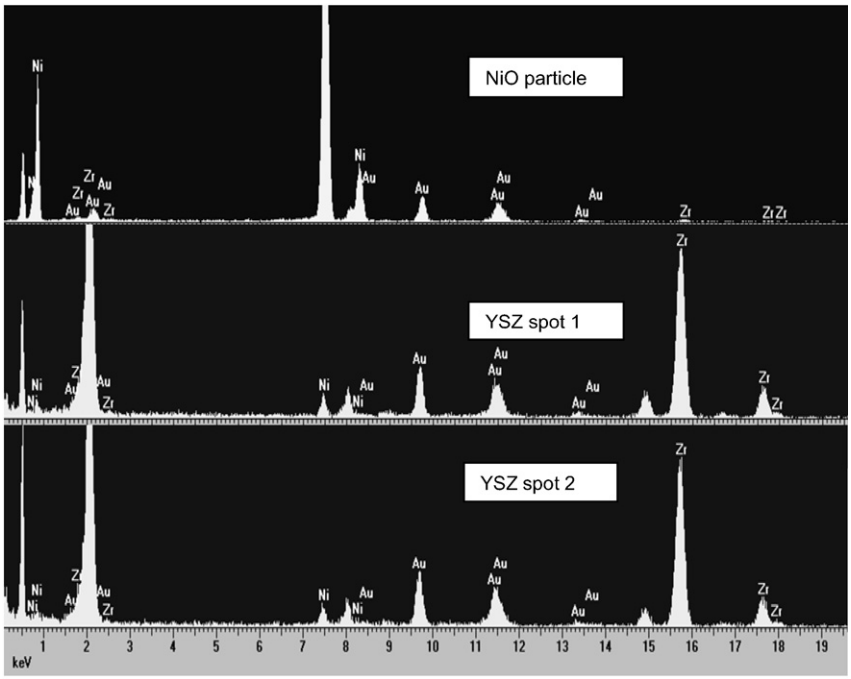

Fig. 8. EDS traces of NiO and YSZ particles showing presence of NiO within the YSZ.

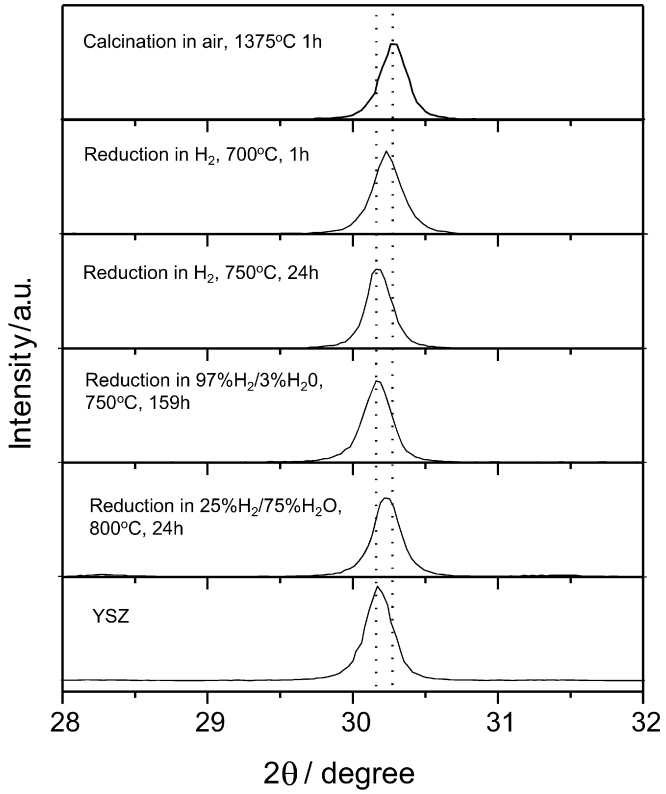

Fig. 9. XRD traces of YSZ and Ni–YSZ showing the effect of different pretreatments on the position of the $(111)_{c,t}$ ZrO_2 peak.

3.2.2. XRD analysis

To help distinguish between surface deposition and dissolution of NiO, XRD analysis of calcined NiO–YSZ was carried out, as shown in Fig. 9. The figure also provides XRD traces of Ni–YSZ following various reductive treatments, along with the spectrum of pure YSZ. We focused specifically on the $(111)_{c,t}$ line of zirconia, which occurs in both the cubic and tetragonal forms with only a very small difference in peak position. The figure shows that the $(111)_{c,t}$ peak for YSZ without Ni is located at $2\theta = 30.14°$. For Ni–YSZ, after calcination, this peak shifted to a higher 2θ value by approximately 0.12°, consistent with a decrease in lattice spacing. This suggests NiO dissolution into the YSZ lattice. For the Ni–YSZ sample that underwent reduction at 700 °C for 1 h, the $(111)_{c,t}$ peak underwent a partial shift back to lower 2θ value, indicating a decrease in dissolved NiO as a result of exolution of Ni from the YSZ. These XRD results are consistent with the findings of Linderoth [28]. After a reduction at 750 °C (with 3% H_2O present in the reducing gas), the $(111)_{c,t}$ peak shifted even further toward unsubstituted YSZ, suggesting near-complete exolution of Ni. With a pretreatment at 800 °C using a 25% H_2–75% H_2O mix, less of a shift toward unsubstituted YSZ was observed, indicating that more NiO was retained within the YSZ despite the higher reduction temperature. This may be due to the high steam concentration retarding reduction or from increased solubility of NiO within the YSZ at the elevated temperature. These results suggest that NiO was initially dissolved in YSZ after calcination, but that under reduction conditions, some Ni exolved from the YSZ. High concentrations of H_2O and elevated temperatures appeared to retard this exolution process.

3.2.3. TEM surface structures of Ni–YSZ after reduction and reaction

Fig. 7 shows the TEM micrographs of the NiO and YSZ particles following high temperature calcination. After a 1-h reduction of Ni–YSZ at 700 °C, a different surface structure appeared, as shown in Fig. 10. In addition to the large particles of Ni and YSZ, many small particles at the surface of the larger YSZ particles can be seen. These particles are pure Ni, as determined by EDS analysis. This appearance of Ni at the surface of YSZ is consistent with the XRD results, indicating that after reduction at 700 °C, small Ni particles exolved from the larger YSZ particles. Fig. 11 shows a TEM micrograph of Ni–YSZ that underwent reduction at 700 °C in H_2, followed by steam reforming at 700 °C for 65 h. For convenience of the TEM analysis, the sample was prepared without YSZ diluent in the catalyst bed, using a feed ratio of $S/C/H_2/N_2 = 3/1/1/5$ and a space velocity of 200,000 cc/g h. In this experiment, the sample reached a lined-out steady-state activity by approximately 50

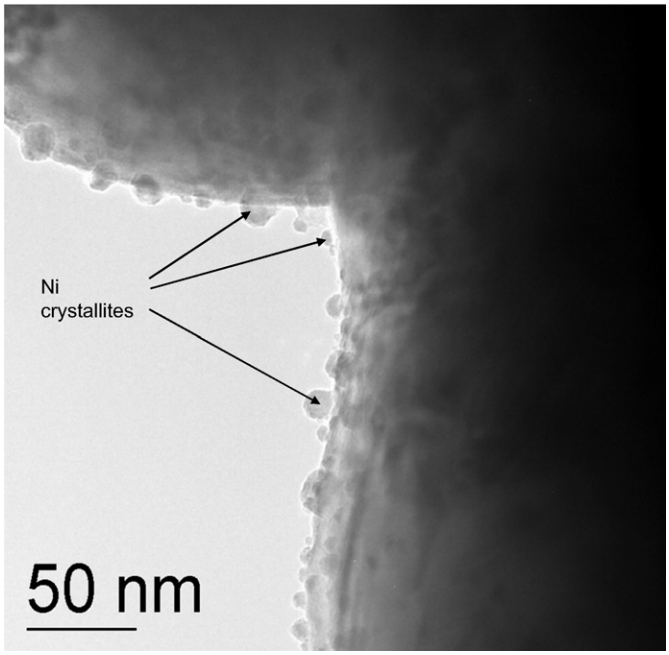

Fig. 10. TEM image of YSZ particle following ramped reduction in hydrogen and hold at 700 °C for 1 h. Small particles are pure Ni.

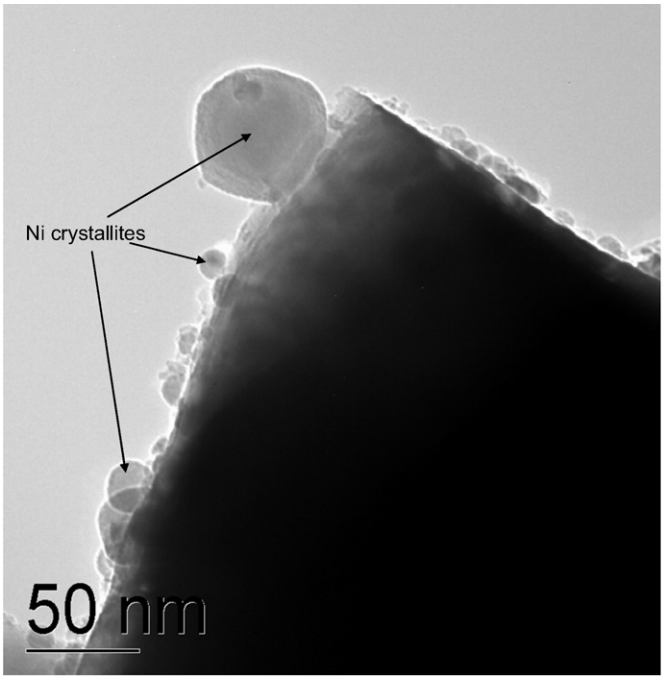

Fig. 11. TEM image of YSZ particle following SMR at 700 °C for 65 h at S/C = 3.

h. The micrograph shows that many of the small Ni particles had sintered. Whereas Ni particle diameters after reduction were typically in the range of 10–20 nm, a broader distribution of particle sizes was seen after reaction, with many in the 30–50 nm range or larger. This loss of surface area as a result of Ni sintering is consistent with the loss of CH_4 conversion.

3.2.4. Catalytic activity

The catalytic activity of Ni–YSZ and its change with time is critical to predicting its reforming performance as a SOFC anode. Because we typically tested small amounts of diluted catalyst (30 mg of active material), subsequent analysis for metal surface area was difficult. Therefore, most calculations of activity were on a per-Ni weight basis. As described earlier, our results indicate catalytic performance consistent with a rate expression that was first-order in methane and zero-order in steam. This is consistent with the findings of Wei for supported Ni catalysts [29],

$$\text{rate} = k[\text{CH}_4]. \tag{1}$$

Despite operating at high space velocities, we had sufficiently high conversions such that kinetics based on differential conditions could not generally be applied. Thus, we applied integral kinetics, in which k above was determined from

$$k = (1/\tau)\ln\bigl(1/\bigl(1 - [\text{X}_{\text{CH}_4}]\bigr)\bigr), \tag{2}$$

where τ is the residence time and X_{CH_4} is the measured methane conversion. Rates for Ni–YSZ under various test conditions and degrees of aging are provided in Table 1. The table shows that the change in k from fresh to lined-out activity frequently reached or exceeded an order of magnitude.

Table 2 provides the comparative rates of Ni–YSZ and reduced bulk NiO calculated from the activity curves shown in Fig. 6. In this case, larger quantities of samples were used, allowing hydrogen chemisorption to quantify surface Ni sites after both reduction and reaction. The Ni–YSZ sample, which contains the same amount of Ni as the bulk NiO, was approximately 2.5 times as active in terms of initial activity and nearly 2 times as active after lineout. Thus, the exolved Ni crystallites provided a significant contribution to the overall activity throughout the course of the test. Table 2 also gives the average turnover frequencies calculated for Ni–YSZ and reduced bulk NiO. Both samples exhibited much higher initial turnover frequencies compared with the values after lineout. This indicates that some very active sites were initially present on both samples but were short-lived. The H_2 chemisorption method is not effective in distinguishing and quantifying these very active sites; thus, initial average turnover frequencies may have only limited value. For the lined-out materials, which contain far fewer highly active sites, the turnover frequencies were nearly equivalent. The fresh activity results indicate that there is structure-sensitivity to methane steam reforming over Ni, likely due to the presence of highly active, coordinatively unsaturated sites. With the aged samples, with Ni particles typically $\geqslant$30–50 nm, there appears to be little evidence for structure sensitivity. This is consistent with the observations of Sehested [30].

3.3. Activation energy measurements

The reported activation energies for methane steam reforming over Ni–YSZ have varied widely, from as high as has 230 kj/mol [31] to as low as 58 kj/mol [32]. For our measurements, in one set of experiments, a Ni–YSZ sample was reduced at 800 °C and exposed to methane steam reforming ($S/C/H_2 = 3/1/1$) at 800 °C until lineout was achieved. This sample was subsequently tested for methane steam-reforming activity in the range 700–800 °C to estimate the activation energy for reaction, as shown in Fig. 12. The value obtained was 124 kJ/mol. In another experiment, Ni–YSZ was reduced and lined-out at 700 °C, followed by measuring conversion at 650–725 °C; a lower value of 113 kj/mol was obtained. These values are in reasonable agreement with, but slightly higher than the value of 95 kj/mol reported by Ahmed and Foger over Ni–YSZ [25] and 102 kj/mol by Wei over a more conventional Ni/MgO catalyst [29]. On the other hand, when the temperatures used to measure activation energy (up to 800 °C) significantly exceeded the temperature at which the Ni–YSZ was initially reduced and stabilized (700 °C), reliable activation energy data could not be obtained. The activity at 800 °C was unstable and decreased slightly with time (over a three hour measurement period), suggesting

Table 1
Comparative activities of Ni–YSZ samples following various pretreatment procedures, with subsequent testing at 700 °C and S/C/H = 3/1/1

Pretreatment reduction (T, t); other	Reforming test conditions (T, S/C/H)	Time on stream (h)	CH_4 conversion	Rate (mol CH_4/g_{cat} h)
Ramp to 700 °C, hold 1 h	700, 3/1/1	0	0.773	4.42
		145	0.081	0.25
Ramp to 700 °C, hold 1 h; H_2O/H_2 = 1/2, 7 h	700, 3/1/6	0	0.185	0.31
		19	0.105	0.17
Ramp to 700 °C, hold 1 h	700, 1/1/1	0	0.42	1.64
		60	0.30	1.07
Ramp to 1000 °C, hold 1 h	700, 3/1/1	0	0.46	1.88
		70	0.116	0.38
Ramp to 750 °C [3% H_2O/97% H_2], hold 150 h	700, 3/1/1	0	0.51	2.18
		70	0.175	0.54

Table 2
Comparison of initial and lined out methane steam reforming activities and turnover frequencies for Ni–YSZ and bulk Ni at 750 °C and S/C/H = 3/1/1

Material	Age (h)	CH_4 conversion	Rate (mol CH_4/g Ni h)	Metal surface area (μmol Ni/g Ni)	Turnover frequency (s^{-1})
Ni–YSZ	Fresh (0)	0.76	6.97	25.2	76.8
	43	0.12	0.63	9.6	18.2
Ni (bulk)	Fresh (0)	0.42	2.71	7.4	101.6
	20	0.07	0.34	5.0	18.9

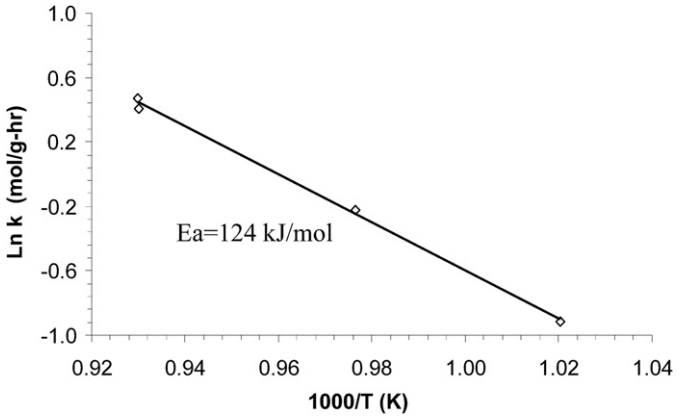

Fig. 12. Activity vs temperature plot (range 700–800 °C) for Ni–YSZ following initial reduction and lineout under steam reforming at 800 °C.

that the material was still undergoing microstructural changes and additional sintering was occurring. This observed decrease in activity at higher temperatures with an unstabilized sample may help explain the nonlinearity of the Arrhenius plots reported by Dicks [18].

3.4. CO selectivity and WGS activity

In addition to measurement of methane conversion, chromatographic analysis also allowed measurement of CO and CO_2 concentrations in the reformate. It is frequently assumed that the water–gas shift reaction is fast compared with reforming, so that at any given time during reaction, the composition of CO, CO_2, H_2O, and H_2 are in equilibrium. Frequently, we encountered a different result. Fig. 6 includes CO selectivity data in addition to the CH_4 conversion performance discussed earlier. The CO selectivity shown is defined as $CO/(CO + CO_2)$. The results shown are typical; a decrease in methane conversion activity was accompanied by an increase in CO selectivity.

For comparison, thermodynamic CO selectivity was calculated using HSC software [33]. The predicted CO selectivity is a function of CH_4 conversion, reflecting more H_2 and less H_2O available with increasing conversion. For the initial methane conversions of 76 and 42% for the Ni–YSZ and Ni-only samples, respectively, the calculated CO selectivities were 53 and 42%, in near agreement with measured values. For the lined-out catalysts (14 and 7% conversion, respectively), however, the predicted CO selectivities were 28 and 24%. These lower predicted selectivities reflect the greater amount of steam available to drive the CO shift. The actual measured CO selectivities were much higher than these calculated values, approximately 80%. Higher CO selectivity is consistent with lower water–gas shift activity. Thus, under the conditions of our tests, only the freshly reduced catalysts, which appear to contain highly active sites (based on the turnover frequencies reported in Table 2), were capable of reaching thermodynamic CO equilibrium. As the catalysts deactivated, there appears to be insufficient catalytic activity to establish water–gas shift equilibrium. This suggests that the water–gas shift reaction can be limited with these catalysts under the high space velocities used.

4. Discussion

The activity of the Ni–YSZ anode is important in determining the electrical performance and temperature distribution of an operating fuel cell when CH_4 is contained in the feed. We have found that the reforming activity is a result of two distinct types of Ni particles. The first type is provided by the original source (bulk) NiO, which is a rather coarse material with particle sizes generally in the range of 0.3–2.0 μm. The second derives from NiO that dissolves into the YSZ to form a solid solution, and subsequently exolves during reductive pretreatment:

$[NiO] = [NiO]_{YSZ}$
(dissolution of NiO in YSZ during sintering in air),
$[NiO]_{YSZ} = [Ni]$
(exolution of Ni during reduction and operation).

The exolved Ni particles, formed at the YSZ surface, are small, typically 10–20 nm in diameter, depending on the temperature and time of reduction. Although comprising only a small fraction of the total Ni in the sample, these small Ni particles contribute significantly to the total activity. Previous studies by Finnerty [34] indicated that based on TPR studies, two types of NiO exist in Ni–YSZ: larger, relatively free particles and smaller particles more strongly associated with the support. The impact of the two different Ni particle types on reforming activity was not evaluated in that study. Our interpretation is that the higher-temperature TPR peak observed by Finnerty is associated with the Ni reduction occurring during exolution of NiO from YSZ. We also note that the

exolution of Ni from the YSZ is retarded by the presence of high levels of steam in the reducing gas.

These small particles are unstable toward sintering under reaction conditions in steam-rich reducing environments. Previous work has shown that sintering slows and particle size stabilizes after approximately 200 h, consistent with our results [35]. The method of sintering depends on temperature, and it appears likely that both coalescence and vapor-phase migration occur [36]. The larger NiO particles also apparently undergo sintering, or at least surface restructuring. This latter effect must arise from the instability of the initially reduced bulk NiO, which undergoes a volume contraction of ∼40% [37]. This rapidly contracted sample likely contains faults, high-surface energy sites, and other defects that have short lifetimes during reforming. As a result of the sintering of both types of Ni particles, overall methane-reforming activity can decrease with time by an order of magnitude or even more, until the system eventually reaches a steady state.

The method by which NiO becomes incorporated into the YSZ is not fully understood. The dissolution of NiO to form a solid solution [38] must occur during the calcination step, but there must be a mechanism by which NiO becomes available at the surface of the YSZ in a form ready for dissolution. It is possible that (i) NiO particulates generated by the milling procedure are initially present on the surface of the YSZ and are available for dissolution; (ii) NiO is provided through contact points between bulk NiO and YSZ, or (iii) NiO vapor-phase transport is occurring during the calcination procedure. At present, we do not have sufficient information to allow us to select among these possibilities. We are also unable to determine from our methods the total concentration of NiO in the YSZ or the presence of NiO concentration gradients within the YSZ particle. Chen has estimated the concentration of NiO in 5YSZ at approximately 3 mol% [39], whereas Kuzjukevics has estimated NiO in 6YSZ at <5 mol% [40]. Other work suggests that the NiO concentration in YSZ is closer to 1 mol% [41]. Although it seems likely that any NiO dissolved into the YSZ would be located near the external surface of the YSZ particle, given the relatively short sintering time (ramped and held for 1 h at 1375 °C), the XRD data indicate otherwise. The sintered Ni–YSZ sample showed a shifted $(111)_{c,t}$ zirconia peak, suggestive of a more homogeneous distribution of NiO, rather than a broadened peak indicative of a combination of NiO-rich and NiO-free regions. This is consistent with the work of Delaforce, who indicates that NiO migration within YSZ can be rapid [41].

This particular catalytic system comprises a rather unique mix of large and small Ni crystallites. However, the aging behavior of the freshly reduced bulk Ni sample is surprisingly similar to that of the freshly reduced Ni–YSZ sample, despite the apparent lack of small Ni crystallites in the former that can undergo sintering. As described earlier, the reduction of the bulk Ni particles results in a lattice contraction, possibly with the generation of cracks and voids that provide Ni sites with high activity and coordinative unsaturation but poor stability under reaction conditions. This suggests the presence of structure sensitivity for methane steam reforming over Ni when these highly active sites are present, but they are apparently unstable under the reaction conditions. (A similar argument may hold with respect to water–gas shift activity.) Our surface characterization is unable to quantify these types of sites, and thus average turnover frequencies with freshly reduced catalysts may have little meaning (similarly with the freshly reduced Ni–YSZ). On the other hand, both aged sets of samples are unlikely to contain such highly active sites, and the measured turnover frequencies are quite similar. This indicates that 30–50 nm (and larger) Ni crystallites, which are substantially present only in the Ni–YSZ, show no evidence for higher activity as a result of structure sensitivity.

5. Conclusion

The catalytic activity and activity maintenance of nickel–yttria stabilized zirconia anode materials, prepared by co-milling and co-sintering a mixture of NiO and 5YSZ powders with subsequent ramped reduction in H_2, was measured for methane steam reforming at 700–750 °C using a steam-methane–hydrogen co-feed and a steam/carbon ratio of 3. Two contributions to the catalytic activity were detected—from large bulk nickel particles derived from the source material and from small Ni crystallites located at the surface of the YSZ particles. During the high-temperature sintering step, NiO dissolved into the YSZ to form a solid solution, and then exolved to form small Ni particles under pretreatment in hydrogen. Both types of particles contributed to the overall methane-reforming activity. With time on stream, methane conversion decreased significantly, due to sintering of both the small and bulk Ni particles. Turnover frequencies per exposed Ni metal site, as measured by H_2 chemisorption, were much higher with the freshly reduced catalysts for both the bulk Ni and Ni–YSZ samples, likely due to some highly active sites that were unstable under reaction conditions. This indicates the presence of a structure-sensitivity effect with Ni arising from such sites. The sintered and lined-out samples exhibited comparable per-site activity, indicating that structure sensitivity for methane steam reforming was no longer present. Catalysts reduced and aged at higher temperatures were less active and revealed modestly higher activation energy. The lined-out Ni–YSZ catalysts typically showed greater-than-equilibrium CO selectivity, indicating that the water–gas shift activity was not fast relative to steam reforming. The results indicate a strong effect of the Ni microstructural evolution on the activity of Ni–YSZ for the steam reforming of methane. Reduction procedure, reactant composition, temperature of reforming, and time on stream all can affect the Ni microstructure and thus the reforming activity, and Chunshe Cao for assistance with the kinetic analysis.

Acknowledgments

Support for this work by the US Department of Energy, Office of Fossil Energy, through the Solid State Energy Conversion Alliance (SECA) program is gratefully acknowledged. A portion this work was performed in the PNNL Environmental Molecular Sciences Laboratory, a national scientific user facility sponsored by the US Department of Energy's Office of Biological and Environmental Research. We thank Vince Sprenkle, Kerry Meinhardt, and Jeff Bonnett at PNNL for supplying the Ni–YSZ samples and engaging in fruitful discussions.

References

[1] P. Singh, R.J. Ruka, R.A. George, in: Proceedings of the 24th Intersociety Engineering Conference, vol. 3, 1989, p. 1553.
[2] J. Meusinger, E. Reinsche, U. Stimming, J. Power Sources 71 (1998) 315.
[3] A.L. Dicks, J. Power Sources 71 (1998) 111.
[4] C.M. Finnerty, N.J. Coe, R.H. Cunningham, R.M. Ormerod, Catal. Today 96 (1998) 137.
[5] A. Gunji, C. Wen, J. Otomo, T. Kobayashi, K. Ukai, Y. Mizutani, H. Takahashi, J. Power Sources 131 (2004) 285.
[6] T. Iida, M. Kawano, T. Matsui, R. Kikuchi, K. Eguchi, J. Electrochem. Soc. 154 (2) (2007) B234.
[7] W. Lehnert, J. Meusinger, F. Thom, J. Power Sources 87 (2000) 57.
[8] P. Aguiar, N. Lapeña-Rey, D. Chadwick, L. Kershenbaum, Chem. Eng. Sci. 56 (2001) 651.
[9] M. Boder, R. Dittmeyer, J. Power Sources 155 (2006) 13.
[10] T. Ackmann, L.G.J. de Haart, W. Lehnert, D. Stolten, J. Electrochem. Soc. 150 (6) (2003) A783.
[11] E.S. Hecht, G.K. Gupta, H. Zhu, A.M. Dean, R.J. Kee, L. Maier, O. Deutschmann, Appl. Catal. A 295 (2005) 40.
[12] E. Achenbach, E. Riensche, J. Power Sources 52 (1994) 283.

[13] P. Aguiar, D. Chadwick, L. Kershenbaum, Chem. Eng. Sci. 57 (2002) 1665.
[14] P. Aguiar, D. Chadwick, L. Kershenbaum, Chem. Eng. Sci. 59 (2004) 87.
[15] L.T. Lim, D. Chadwick, L. Kershenbaum, Ind. Eng. Chem. Res. 44 (2005) 9609.
[16] V.M. Janardhanan, O. Deutschmann, J. Power Sources 62 (2006) 1192.
[17] A.L. Dicks, J. Power Sources 71 (1998) 111.
[18] A.L. Dicks, K.D. Pointon, A. Siddle, J. Power Sources 86 (2000) 523.
[19] S. Bebelis, A. Zeritis, C. Tiropani, S.G. Neophytides, Ind. Eng. Chem. Res. 39 (2000) 4920.
[20] N. Nakagawa, H. Sagara, K. Kato, J. Power Sources 92 (2001) 88.
[21] R. Peters, R. Dahl, U. Klüttgen, C. Palm, D. Stolten, J. Power Sources 106 (2002) 238.
[22] S.H. Clarke, A.L. Dicks, K. Pointon, T.A. Smith, A. Swann, Catal. Today 38 (1997) 411.
[23] A.L. Lee, R.F. Zabransky, W.J. Huber, Ind. Eng. Chem. Res. 29 (1990) 766.
[24] A.L. Dicks, K.D. Pointon, A. Swann, in: P. Stevens (Ed.), Proceedings of the 3rd European SOFC Forum, 1998, p. 249.
[25] K. Ahmed, K. Foger, Catal. Today 63 (2000) 479.
[26] J. Sehested, J. Catal. 217 (2003) 417.
[27] J. Sehested, J.A.P. Gelten, I.N. Remediakis, H. Bengaard, J.K. Norskøv, J. Catal. 223 (2004) 432.
[28] S. Linderoth, N. Bonanos, K.V. Jensen, J.-B. Bilde-Søren, J. Am. Ceram. Soc. 84 (110) (2001) 2652.
[29] J. Wei, E. Iglesia, J. Catal. 224 (2004) 370.
[30] J. Sehested, Catal. Today 111 (2006) 103.
[31] J. Divisek, W. Lehnert, J. Meusinger, U. Stimming, in: U. Stimming, S.C. Singal, H. Tagawa, W. Lehnert (Eds.), Proceedings of the Fifth International Symposium of SOFCs, The Electrochemical Society, 1997, p. 993.
[32] R. Odegaard, E. Johnsen, H. Karoliussen, in: M. Dokiya, O. Yamamoto, H. Tagawa, S.C. Singhal (Eds.), Proceedings of the Fourth International Symposium on SOFCs, The Electrochemical Society, 1995.
[33] HSC Chemistry 5, licensed from Outokumpu Research Oy, Pori, Finland.
[34] C.M. Finnerty, N.J. Coe, R.H. Cunningham, R.M. Ormerod, Catal. Today 96 (1998) 137.
[35] J. Sehested, A. Carlsson, T.V.W. Janssens, P.L. Hansen, A.K. Datye, J. Catal. 197 (2001) 200.
[36] F.B. Rasmussen, J. Sehested, H.T. Teunissen, A.M. Molenbroek, B.S. Clausen, Appl. Catal. A 267 (2004) 165.
[37] S. Modena, S. Ceschini, A. Tomasi, D. Montinaro, V.M. Sglavo, J. Fuel Cell Sci. Technol. 3 (2006) 487.
[38] H. Kondo, T. Sekino, T. Kusunose, T. Nakayama, Y. Yamamoto, K. Niihara, Mater. Lett. 57 (2003) 1624.
[39] S. Chen, P. Shen, D. Gan, Mater. Sci. Eng. A. 158 (1992) 251.
[40] A. Kuzjukevics, S. Linderoth, Mater. Sci. Eng. A 232 (1997) 163.
[41] P.M. Delaforce, J.A. Yeomans, N.C. Filkin, G.J. Wright, R.C. Thomson, J. Am. Ceram. Soc. 90 (3) (2007) 918.